Bio-inspired design for enhanced damage tolerance of self-reinforced polypropylene/carbon fibre polypropylene hybrid composites

Lorenzo Mencattelli[a], Jun Tang[b], Yentl Swolfs[b], Larissa Gorbatikh[b], Silvestre T. Pinho[a]

[a] *Department of Aeronautics, Imperial College London South Kensington, SW7 2AZ, UK*

[b] *Department of Materials Engineering, KU Leuven Kasteelpark Arenberg 44, 3001 Leuven, BE*

Abstract

In this work, we investigate the toughness of an inter-layer Self-Reinforced Polypropylene/ Carbon Fibre Polypropylene (SRPP/CFPP) cross-ply hybrid composite and devise strategies to improve two aspects of its damage tolerance: (i) increasing damage diffusion and hence energy dissipation capability and (ii) enhancing the impact damage tolerance. To this end, we locally engineered the microstructure of the composite via introducing discontinuities in the form of laser-cuts across the fibres of the CFPP plies. We tailored two patterns of laser-cuts to meet each specific damage tolerance requirement. We designed baseline specimens and specimens with engineered microstructures to conduct Double Edge Notched Tensile (DEN-T) and low velocity drop-weight penetration impact tests. We used the Essential Work of Fracture (EWF) method to provide a measure of fracture toughness and energy dissipation performances of the hybrid composites. The DEN-T tests show that hybridising PP tapes with continuous carbon fibres results in a tough material — 213 kJ/m^2. Engineering the microstructure of DEN-T samples has successfully delocalised strain concentrations and extensively diffused dam-

Email addresses: l.mencattelli@imperial.ac.uk (Lorenzo Mencattelli), jun.tang@kuleuven.be (Jun Tang), yentl.swolfs@kuleuven.be (Yentl Swolfs), larissa.gorbatikh@kuleuven.be (Larissa Gorbatikh), silvestre.pinho@imperial.ac.uk (Silvestre T. Pinho)

age. The activation of dissipative mechanisms, such as pull-outs of CF bundles, has led to a great increase in energy dissipation capability of the structure — 90% increase in the slope of the Specific Work of Fracture (SWF) with respect to the baseline. Engineering the microstructure of impact samples has led to enhanced impact damage tolerance, with a more ductile impact response, increased energy dissipation at a sub-critical level and delayed critical failure.
Keywords: A: Hybrid, B: Damage tolerance, B: Fracture toughness, D: Failure

1. Introduction

SRPP is well known for its good recyclability and processability, outstanding impact resistance [1, 2], high strain to failure [2] and high fracture toughness [3]. However, the low stiffness and yielding point of SRPP have hindered its use in various structural applications. Hybridising carbon fibres with SRPP provides a good combination of reasonable stiffness and high strain to failure [4, 5]. However, the use of carbon fibres increases the brittleness of the composite [5–8], hence compromising the excellent damage tolerance of the SRPP.

The majority of the literature on SRPP/CFPP has focused on the tensile [5–9] and impact behaviour [7, 9] of various SRPP/CFPP hybrid composites. In comparison, to the knowledge of the authors, no research has yet focused on investigating original strategies to improve the damage tolerance of SRPP/CFPPs.

Studies on the tensile behaviour of continuous carbon fibre/SRPP hybrid composites have shown that the presence of carbon fibres, even in small volume fraction (3%), tends to localise damage at the carbon fibre layers, with the localisation being more severe as the carbon volume fraction increases [5, 6]. The abrupt failure of the carbon fibres leads to a high energy release rate that generates delamination and unstable damage growth. Tensile tests on discontinuous carbon fibre/SRPP hybrid composites showed that a transition from a ductile to a brittle

behaviour occurs at very low carbon fibre volume fraction (<6.9%) [7]. Penetration impact tests conducted on the same hybrid composites showed that increasing the volume fraction of carbon fibre (>5.5%) decreases the dissipated energy and leads to a brittle mechanical response [7]. In addition, the penetration occurs at lower indentation depths compared to SRPP laminates [7], hence reducing the damage tolerance of the composite. Therefore, hybridising SRPP even with small volume fractions of carbon fibres in an inter-layer configuration leads to a localisation of damage near where carbon fibres fail, hence decreasing the damage tolerance of the structure.

An enhancement in damage tolerance can be achieved via locally engineering the microstructure using a bio-inspired approach. Specifically, the introduction of discontinuities across the load-carrying fibres via tailored laser-cut patterns has been successful in enhancing the damage tolerance of CFRPs [10–14]. Bullegas *et al.* [11] showed that tailoring laser-cut patterns in compact tension tests of cross-ply thin-ply CFRPs can lead to an improvement of the work of fracture of about 460% and to an increase of 43% in energy dissipation of quasi-isotropic thin-ply CFRPs under quasi static indentation. The occurrence of extensive pull-outs was found to be one of the major causes of such a large increase in energy dissipation (up to 64% of the total work of fracture). Narducci *et al.* [12–14] manufactured a nacre-like CFRP microstructure showing that the use of carefully designed discontinuities forming a tiled microstructure can lead to crack deflection, stable failure and damage diffusion under three-point bending of CFRPs and GFRP/CFRP tiled composites.

Based on the above [10–14], as well as on other studies [15, 16], Tang *et al.* [8] showed that introducing discontinuities in the form of laser-cuts in the CF plies of a SRPP/CFPP tensile sample can successfully lead to a smooth and stable tensile response of the hybrid composite. Therefore, the use of discontinuities to locally engineer the microstructure of typically brittle composite materials can be a versa-

tile tool to improve their mechanical and damage tolerance performance.

We therefore decided to design two patterns of discontinuities, via laser-cuts across the load carrying fibres of CFPP plies, to improve two aspects of the damage tolerance of a SRPP/CFPP continuous fibre CP hybrid laminate: (i) increasing damage diffusion and hence energy dissipation and (ii) enhancing the impact damage tolerance. Regarding the former, we assessed the toughness of the hybrid SRPP/CFPP composites and related energy dissipation capability using the Essential Work of Fracture (EWF) method [17–20] and DEN-T tests. Regarding the latter, we conducted penetration low-velocity impact tests to evaluate the performances of the hybrid composites under impact.

For the first time in the literature: (i) we provide a measure of fracture toughness and energy dissipation capability of SRPP/CFPP hybrid composites; (ii) we demonstrate that the use of carefully designed patterns of discontinuities in the CFPP plies of a SRPP/CFPP hybrid composite significantly improves the damage diffusion and hence the energy dissipation capability of the hybrid structure; (iii) we demonstrate that the use of carefully designed patterns enhances the impact damage tolerance of SRPP/CFPP cross-ply structures; (iv) we provide an understanding of the role of pull-outs in the energy dissipation performances of engineered hybrid SRPP/CFPP structures in DEN-T tests; and (v) we prove that patterns of discontinuities can be tailored to meet different damage tolerance requirements within the same structure, while using the same technique to engineer the microstructure and the same material system.

2. Materials and Methods

2.1. Materials

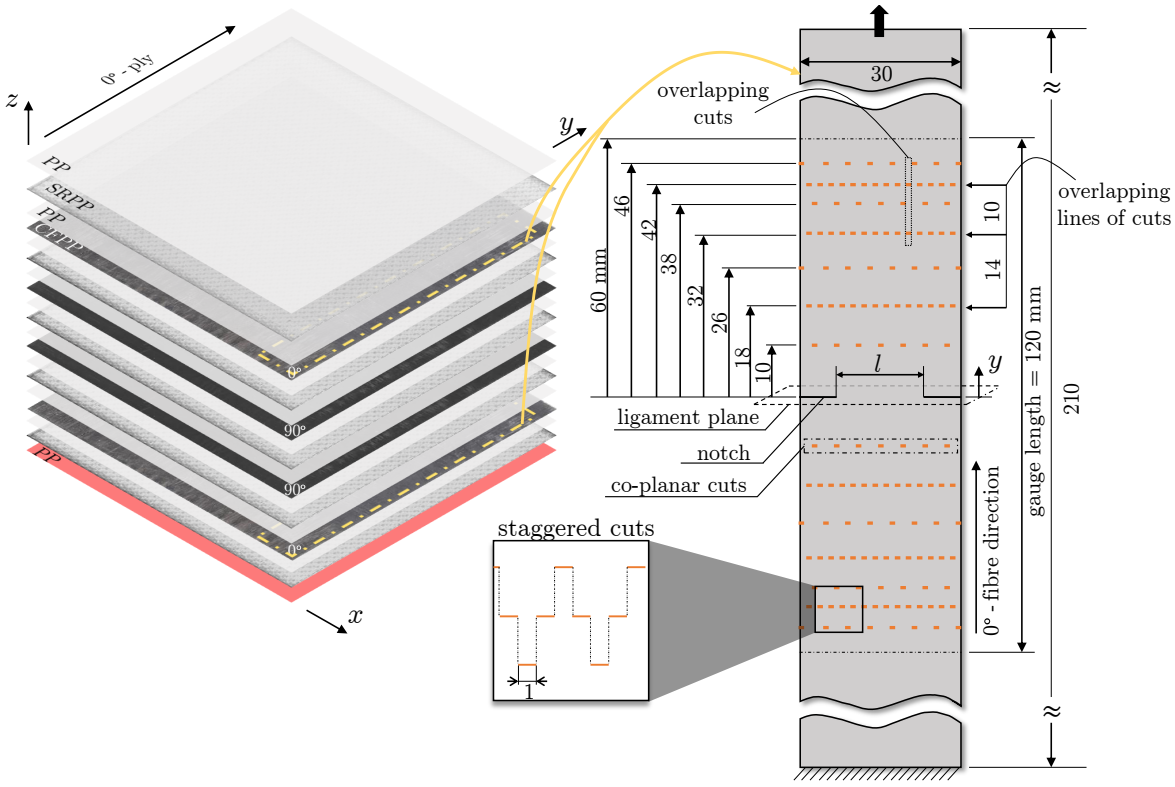
The hybrid SRPP/CFPP laminates comprise three basic constituents:

(i) a PP tape fabric (an overfed twill 2/2 weave with an areal density of 130 g/m^2 supplied by Propex Fabrics GmbH) [21]. The compacted SRPP has a thickness of about 141 µm;

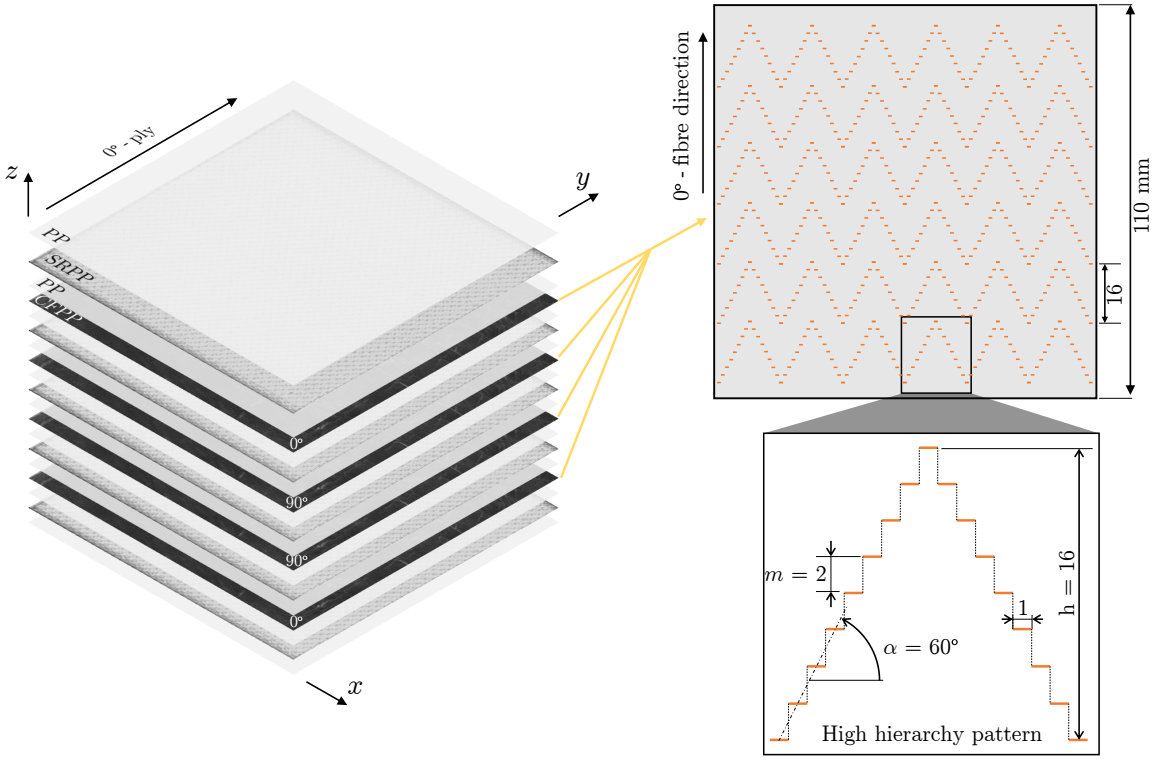
(ii) a PP film of the same PP grade as the SRPP. This is 20 µm thick and 0.92 g/m^2 in areal weight; and

(iii) carbon fibres (T700SC-50C) supplied in a UD spread tow tape from Chomarat. The tape has an areal density of 71.5 g/m^2.

2.2. Design of DEN-T and impact samples



(a) Schematic of DEN-T sample with respective laser-cuts pattern



(b) Schematic of impact sample with respective laser-cuts pattern

We manufactured two pairs of configurations respectively for DEN-T and impact tests. Each pair comprises a baseline (without laser-cuts and identical for both DEN-T and impact tests) and an engineered configuration (with two laser-cut patterns tailored for DEN-T and impact respectively). The stacking sequence and geometry for the DEN-T and impact samples are schematically reported in Figure 1a and Figure 1b respectively. We chose a cross-ply lay-up with the following stacking sequence: $[F/S/F/C_{0°}/F/S/F/C_{90°}/F/S]_{so}$ where F stands for PP film, S for SRPP and C for a layer of UD CFPP prepreg. We preferred a dispersed lay-up over other inter-layer architectures as it improves the impact and tensile performance of the composite [7]. We interleaved a PP film in between each CFPP ply and SRPP ply to guarantee excellent hot compaction quality [8, 22, 23].

In the DEN-T samples, the load is aligned with the fibres of the $C_{0°}$ plies. Furthermore, the $C_{90°}$ plies do very little work during the failure of the laminate compared to the $C_{0°}$ plies [24, 25]. Therefore, in the DEN-T samples, only the $C_{0°}$

plies of the engineered microstructure contains laser-cuts. In the engineered configuration of the impact samples, the C_{90° plies have the same function as the C_{0° plies; therefore, all the carbon fibre plies contain laser-cuts.

In the DEN-T test, we designed the samples such that the C_{0° layers (Figure 1a), i.e. the ones containing laser cuts, were the most external CF layers in the lay-up. This was intended to facilitate observation of the evolution of damage, tapping into the semi-transparency of the SRPP. In addition, to monitor strain evolution via DIC on the DEN-T samples, we substituted one of the two most external PP films with an equivalent (same chemical and mechanical properties) red one (Figure 1a). The reduced transparency of the red PP film allowed for an enhanced contrast with the black speckle pattern, thereby increasing the quality of the strain measurements. For the impact samples, this was not needed because DIC was not performed during tests. Additionally, a translucent PP film enabled a more clear observation of the post-impact damage.

2.3. Design of the laser-cut patterns

2.3.1. DEN-T samples

Figure 1a schematically shows the pattern of laser-cuts designed for the DEN-T samples with engineered microstructure. The pattern can be broken down into three lines of dense laser-cuts, each one neighboured by two coarse lines. The distance between each line of dense cuts and two neighbouring coarse lines decreases as y increases. The resulting pattern is then mirrored about the ligament plane, resulting in a symmetric sample.

The choice of cut length, the spacing between co-planar cuts and the relative spacing between overlapped lines of cuts in Figure 1a follow the outcomes of a previous parametric study conducted by Tang *et al.* [26]. Specifically, Tang *et al.* [26] showed that when the distance between two overlapped cuts increases, the longi-

tudinal tensile stress fully recovers within the discontinuous bundles formed by the two overlapped cuts. Therefore, the two lines of overlapped cuts act independently. Since, in the DEN-T samples, we want to promote interaction between the laser-cuts to maximise damage diffusion, in our design we progressively reduced the distance between two overlapped lines as the distance (y) from the ligament plane increases. This was expected to promote damage initiation in areas of the sample far from the notches and then to grow towards the ligament plane promoting extensive damage diffusion.

2.3.2. Impact samples

Figure 1b schematically shows the pattern of laser-cuts designed for the impact samples with engineered microstructure. The pattern can be broken down into a triangular unit of staggered cuts. The unit is repeated along the transverse direction to form a 'shark-teeth' pattern (inspired by the work of Bullegas *et al.* [27]) and then along the longitudinal direction with a step of 16 mm (see Figure 1b).

We designed the pattern such that there were no continuous fibre bundles in between adjacent cuts (along the transverse direction). This was expected to promote energy dissipation at sub-critical level (i.e. before the occurrence of the load-drop which corresponds to fibre failure). We chose the value of m and α in Figure 1b based on the following considerations: (i) the height of a single unit should be smaller than the striker diameter (ϕ=20 mm) and (ii) at least 4 units should be inside the area delimited by the inner diameter of the clamps (ϕ=40 mm). In the engineered impact samples, a full recovery of stress along the discontinuous bundles during loading was desirable to preserve the load-bearing capability of the engineered hybrid samples. Therefore, we chose a spacing of 16 mm between the staggered units (see Section 2.3.1).

2.4. Manufacturing

We manufactured the hybrid SRPP/CFPP plates in three steps: (i) prepregging of the carbon fibre layer, (ii) laser-cutting of the prepregs and (iii) hot pressing of the hybrid laminate.

In step (i), we hot-pressed a preform of UD carbon fibres sandwiched between two PP films. The same procedure was applied to all the CF plies. The hot pressing of the prepreg was carried out using a Fontijne Grotnes LabPro 400, preheated at 188 °C. We applied a pressure of 5 bar for 5 min and then cooled the prepreg down to 40 °C in 5 min.

In step (ii), we performed the laser-cuts using an Oxford Lasers Diode Pumped Solid State (DPSS) micro-machining system [11, 12]. The high precision laser-milling ensured excellent quality of the cuts and high reproducibility. As shown by the micro-graphs of a representative cut in Figure 2, we managed to produce neat and precise cuts with a constant thickness and a round neat tip of the cut-end with a diameter of 15 µm. The heat generated during cutting, created only a very small thermally affected area around the cut (Figure 2).

In step (iii), we laid-up the hybrid laminate with the stacking sequence of Sec-

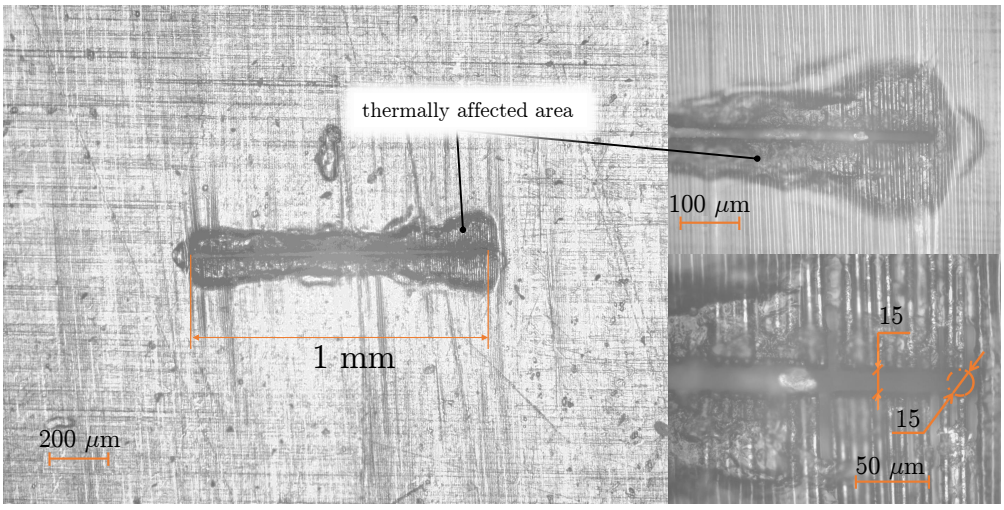


Figure 2: Detail of a laser-cut on a CFPP prepreg.

tion 2.2 and then hot-compacted the plate at 188 °C for 5 min with an applied pressure of 39 bar. The higher pressure was necessary to prevent the shrinkage of PP tapes [8]. The composite plate was then cooled down to 40 °C in 5 min. The final thickness of all the plates ranged between 1.14 mm and 1.18 mm with an estimated carbon volume fraction of 14%. We then cut each plate to the final sample dimensions (210 mm x 30 mm and 110 mm x 110 mm for DEN-T and impact tests respectively) using a bandsaw. Finally, we pre-notched the DEN-T samples using a wire hand-saw and used a razor blade to create a sharp tip with a radius of 125 µm. For each configuration, we manufactured 15 DEN-T samples with nominally evenly-spaced ligament lengths ranging between 5 mm and 19 mm. We further manufactured three nominally-equivalent impact samples for the baseline and engineered configuration, respectively.

2.5. Essential Work of Fracture and DEN-T tests

We performed quasi-static DEN-T tests on an Instron 5567 with a 30 kN load cell and a displacement rate of 2 mm/min using a gauge length of 120 mm. The surface of the samples with the red PP external layer was covered with ink-based black speckles (for DIC). We preferred ink to standard paint-based speckles to avoid premature fracture of the paint due to the high failure strain of SRPP. We used two digital cameras to record both the front and back surfaces of the sample during test. The optimal DIC correlation parameters included a subset size of 19 pixels and a step size of 6 pixels.

We used the EWF method [17–20] on the load vs. displacement diagrams of the DEN-T samples to assess the fracture toughness and energy dissipation capability of the baseline and engineered microstructures. The EWF method, developed for highly ductile polymers such as polypropylene, was preferred to J-Integral and crack tip opening displacement because it provides a clear distinction between the energy dissipated at the ligament plane (essential part) and the work dissipated in

the volume of the sample (non-essential part) [28]. The first corresponds to a measure of fracture toughness while the second correlates with the damage diffusion and energy dissipation performances of the structure.

The EWF method can be applied if the following requirements are met [20]:

- self-similarity of the load vs. displacement diagrams;
- full ligament yielding prior to crack growth; and
- plane stress condition and outer 'plastic' volume proportional to the square of the ligament length (l^2).

where the last two conditions are met if the maximum net section stress is independent of the ligament length (Hill's criterion [29]).

The work of fracture (W_{fracture}) for a DEN-T sample with a certain ligament length is the integral of the load vs. displacement diagram. This can be written as:

$$W_{\text{fracture}} = W_{\text{essential}} + W_{\text{plastic}} \tag{1}$$

with $W_{\text{essential}}$ being the energy dissipated at the fracture plane (ligament plane) and W_{plastic} the energy dissipated in the volume surrounding the ligament plane ('plastic' region). Assuming that the volume of the 'plastic' region scales with l^2, Eq. 1 can be rewritten as follows:

$$W_{\text{fracture}} = w_{\text{essential}} \cdot lt + \beta w_{\text{plastic}} \cdot l^2 t \tag{2}$$

$$w_{\text{fracture}} = \frac{W_{\text{fracture}}}{lt} = w_{\text{essential}} + \beta w_{\text{plastic}} \cdot l \tag{3}$$

where t is the sample thickness and β is the shape factor of the 'plastic' region. $w_{\text{essential}}$ and w_{plastic}, independent of l, are respectively an energy per unit surface

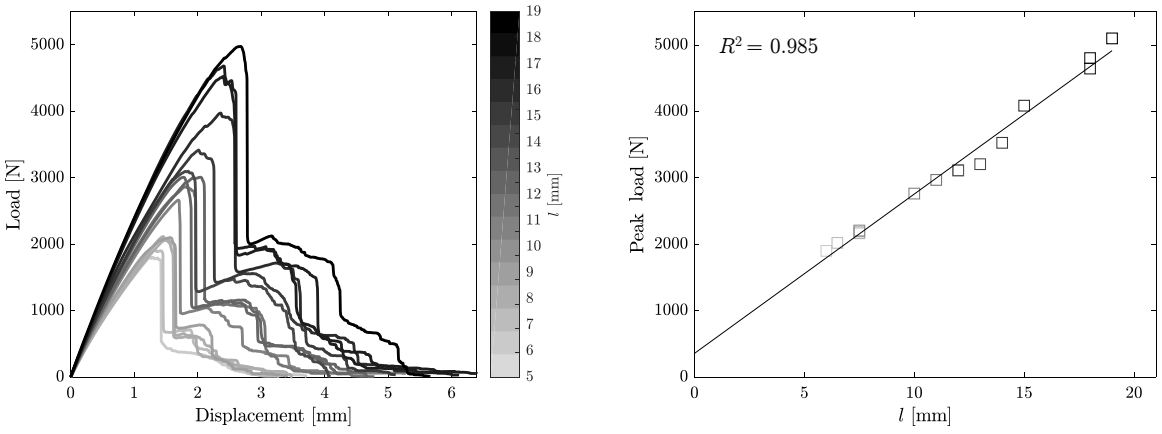
and an energy per unit volume. The intercept of the trend-line of Eq.3 for zero ligament length, $w_{\text{essential}}$, is a measure of fracture toughness. The slope of the trend-line βw_{plastic} is a measure of the damage diffusion and energy dissipation performances of the sample. Since βw_{plastic} is associated to the shape of the 'plastic' region, it depends on both material and geometry of the sample.

2.6. Penetration impact test

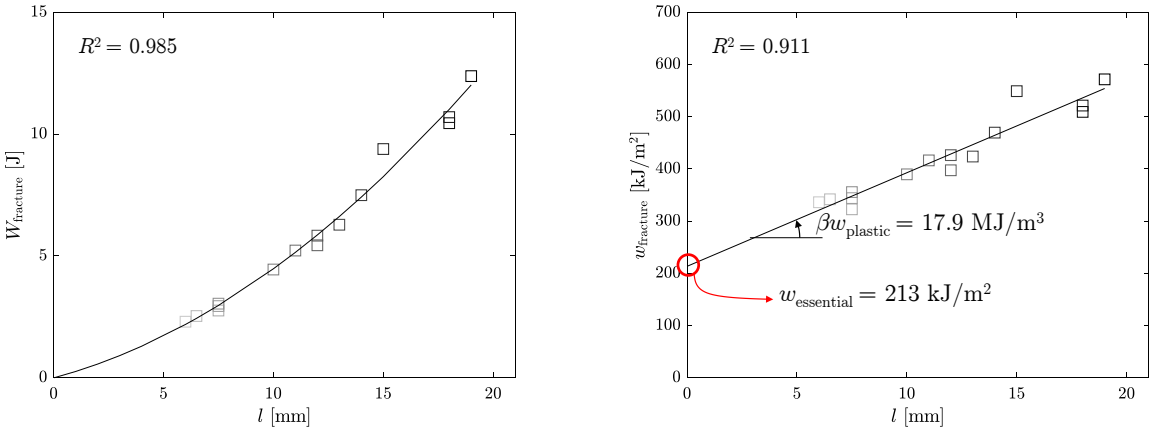
We performed penetration impact tests on square samples of 110 mm x 110 mm clamped with a circular clamp of outer and inner diameter of 60 mm and 40 mm respectively, and a clamping pressure of 1780 kPa. We impacted the samples with an hemispherical (ϕ=20 mm) striker with a weight of 26.17 kg. The striker was dropped from a height of 1 m, thereby impacting the sample with an energy of 256.72 J. The impactor reached the sample surface with a speed of 4.42 m/s.

We quantified the impact performance of the hybrid composites by computing the total dissipated energy and the energy dissipated before the peak load. For each sample, we estimated the two dissipated energies by computing the area under the load vs. displacement diagram, where the displacement represents the displacement of the impactor.

3. Results



(a) (b)



(c) (d)

Figure 3: DEN-T test results for the baseline configuration (a) load vs. displacement diagrams, (b) linear fitting of the peak load with respect the ligament length and associated R^2, (c) quadratic fitting of the work of fracture and associated R^2 and, (d) linear fitting of the specific work of fracture and associated R^2.

For the DEN-T tests of the baseline samples with ligament lengths $5 < l < 19$ mm, Figure 3a shows self-similar load vs. displacement diagrams. Figure 3b shows that the maximum load scales linearly with the ligament length — Hill's criterion applies. In Figure 3c, the work of fracture W_{fracture} is plotted against the ligament length l. This is well fitted by a quadratic polynomial as expected from Eq.2. Figure 3d shows the specific work of fracture w_{fracture} plotted against l. The data are distributed linearly as expected from Eq.3. The trend-line obtained from the linear regression intercepts the zero-ligament axis at 213 kJ/m^2 with a slope of 17.9 MJ/m^3.

The load vs. displacement diagram and photographs of a baseline sample with l=17 mm in Figure 4 show that damage (whitening in Figure 4) was highly localised at the notch tips right before the unstable damage propagation (load-drop).

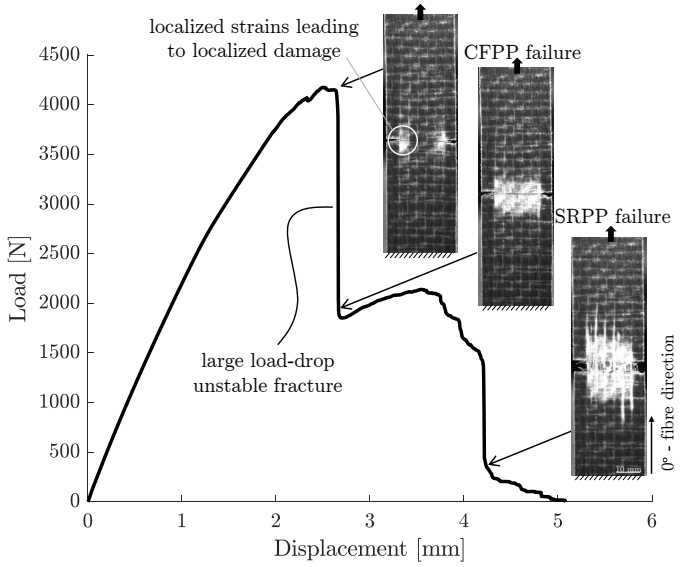


Figure 4: Load vs. Displacement diagram highlighting the fracture process of a DEN-T sample of the baseline configuration with l=17 mm.

For the DEN-T tests of the engineered configuration, Figure 5a shows the load vs. displacement diagrams of the engineered samples (together with those of the baseline). The engineered microstructure, despite a consistent reduction in the maximum load achieved during the test, showed a gradual Load vs. Displacement response. In addition, the engineered microstructure reached higher loads than the baseline during damage growth (after the load drop occurred in the baseline) and higher ultimate displacements, as shown in Figure 5b. Specifically, for $l > 16$ mm, the increase in failure displacement was 190% higher than the displacement at the onset of unstable damage growth in the baseline configuration (CFPP failure) and 50% higher than the displacement calculated at the final failure of baseline samples with similar ligament lengths.

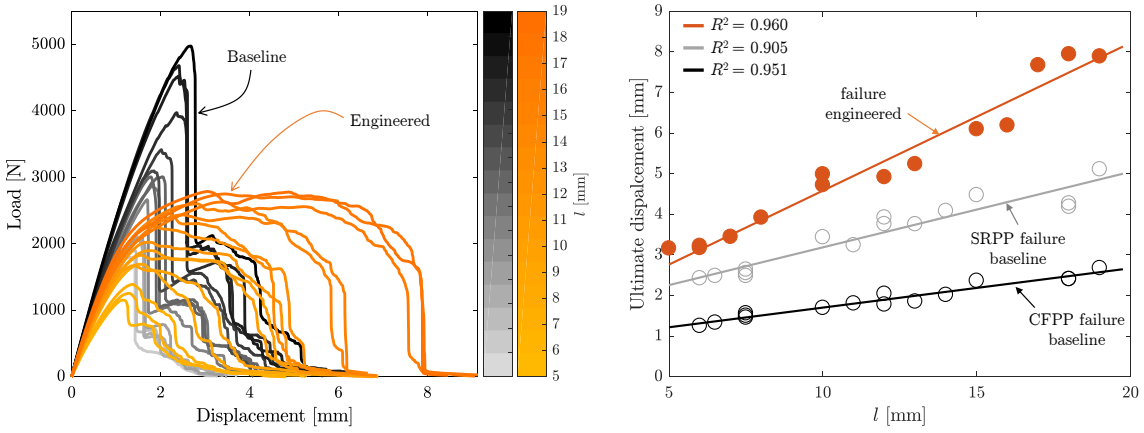


Figure 5: Comparison between (a) the load vs. displacement diagrams of the baseline and the engineered structure and (b) failure displacement for different ligament lengths of the baseline and engineered structures. The black line refers to the ultimate displacement at the CFPP failure of the baseline (load-drop) while the grey line refers to the ultimate displacement at the SRPP failure (displacement at 90% drop of the peak load) of the baseline.

Figure 6 shows the load vs. displacement diagram and photographs of an engineered DEN-T sample with l=17 mm highlighting the highly diffused damage occurring in the engineered microstructure.

Figure 7 shows the DIC maps of an engineered sample with l=18 mm. The graphs in Figure 7b represent the tensile strain ε_y evaluated along the blue line in Fig-

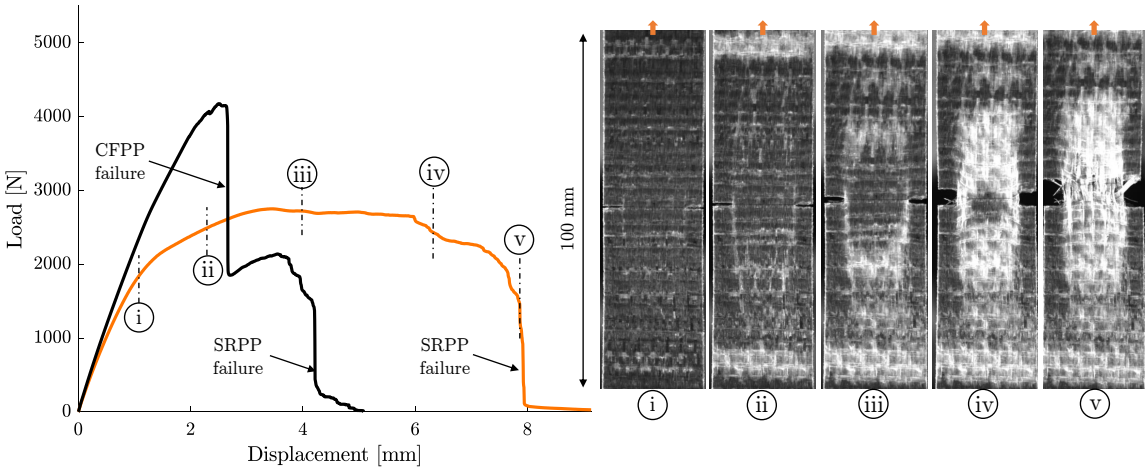


Figure 6: Load vs. Displacement diagram highlighting the fracture process of a DEN-T sample of the engineered configuration with l=17 mm.

ure 7a. The large peaks, which correspond to high strain regions, match very well with the physical position of the laser-cuts along the sample.

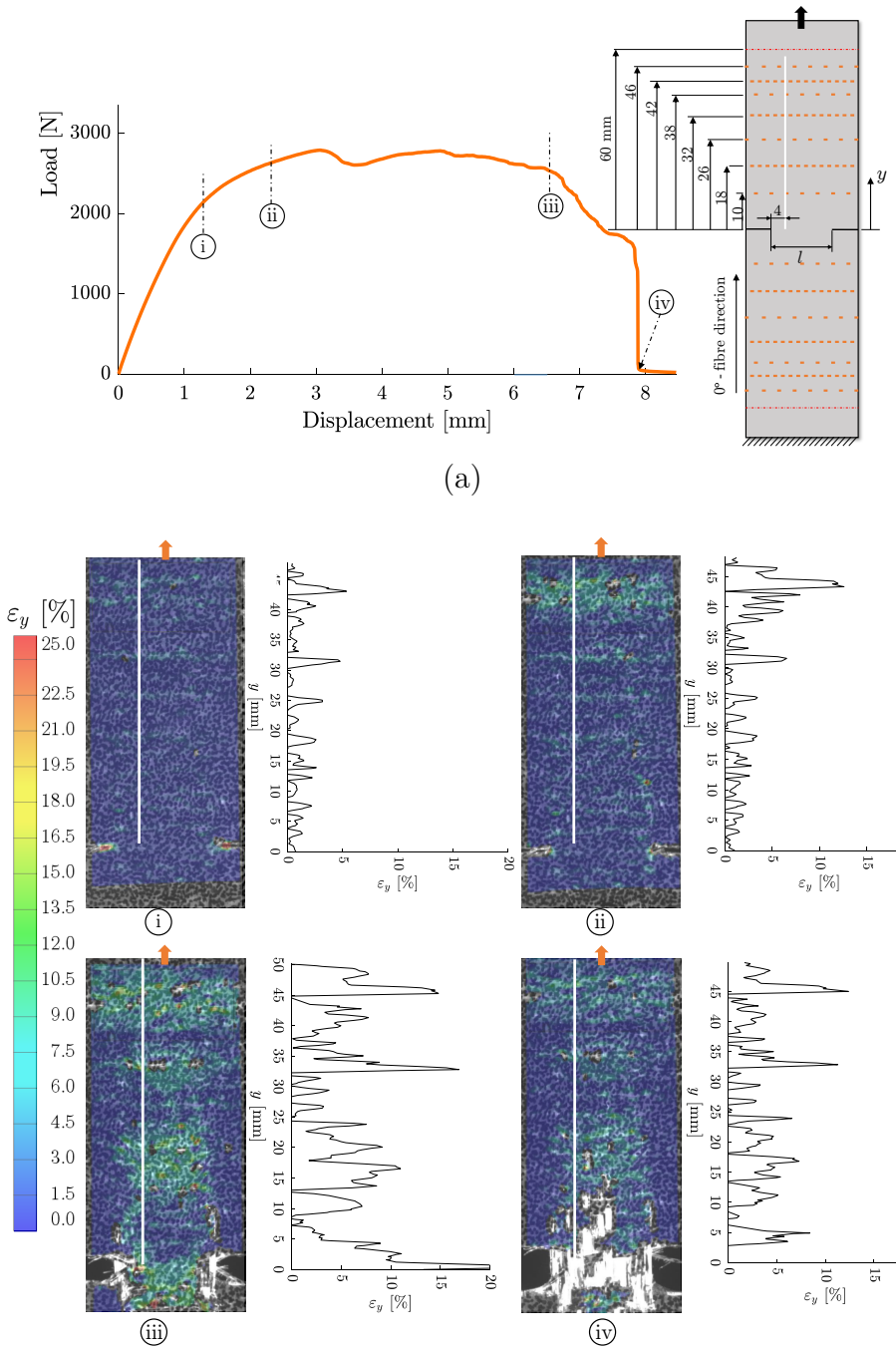
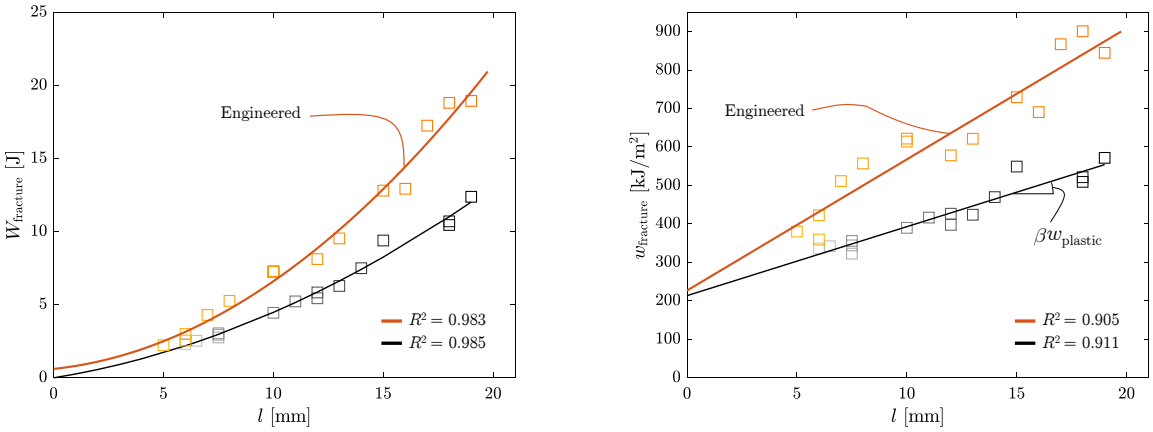


Figure 7: (a) load vs. displacement of a DEN-T sample with engineered microstructure and $l = 18mm$ and schematic of the sample. (b) ε_y obtained from DIC of the DEN-T sample shown in (a) taken along a longitudinal path at different instances during test. For clarity, we report only half of the sample in each DIC map.



(a) (b)

Figure 8: Comparison between (a) the work of fracture and (b) specific work of fracture of baseline and the engineered microstructure.

Figures 8a and 8b respectively show a comparison between the work of fracture and the essential work of fracture of the baseline and engineered configurations. Specifically, Figure8b highlights the large increase in the slope of the specific work of fracture of the engineered configuration, 90% higher than that of the baseline.

Figure 9 shows the load vs. displacement diagrams of the penetration impact tests for the baseline and engineered microstructures. The load-drop of the engineered samples was delayed to larger applied displacements. The increase was found to be 26% on average with respect to the baseline in Figure 10a, and to be statistically significant (p-value = 0.0305, calculated with the One-sample t-test and a standard 5% significance level). In addition, Figure 9 shows that the engineered microstructure preserved the load-bearing capability of the baseline. The energy dissipated prior to the load drop in Figure 10b was found to be on average 42.7% higher for the engineered configuration than for the baseline configuration, and to be statistically significant (p-value = 0.0005). The total dissipated energy was very similar for the two configurations with a statistically non-significant average difference of 3.2% (p-value = 0.178).

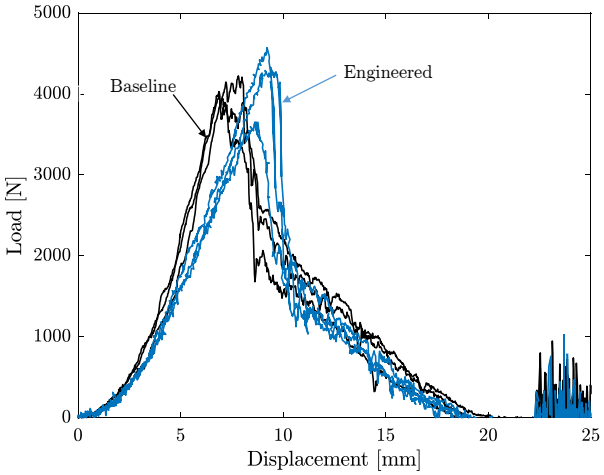


Figure 9: Load vs. Displacement of the baseline and the engineered SRPP/CFPP hybrid composite.

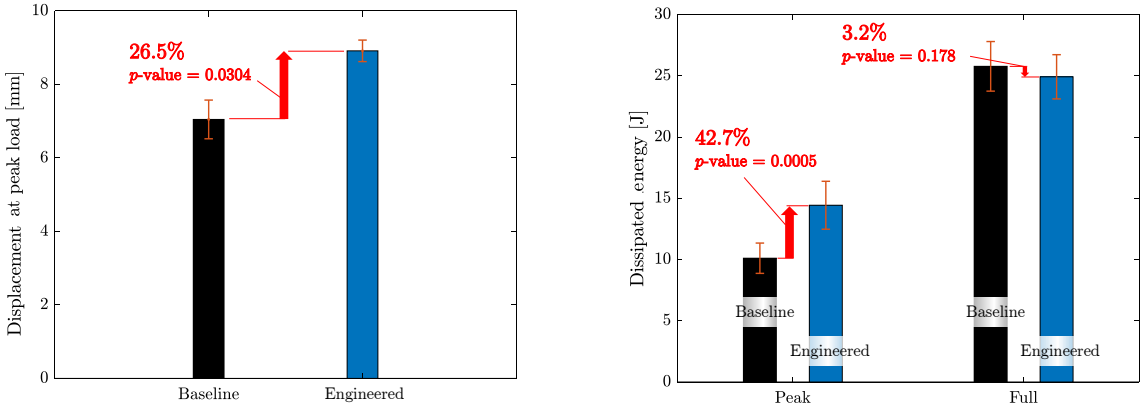
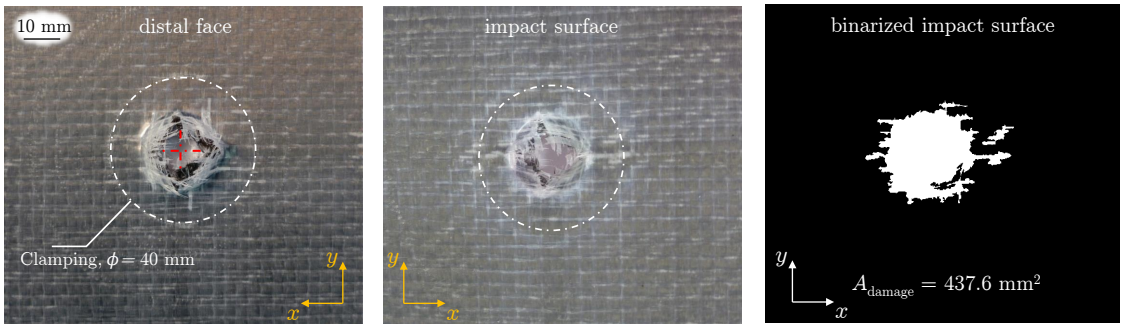


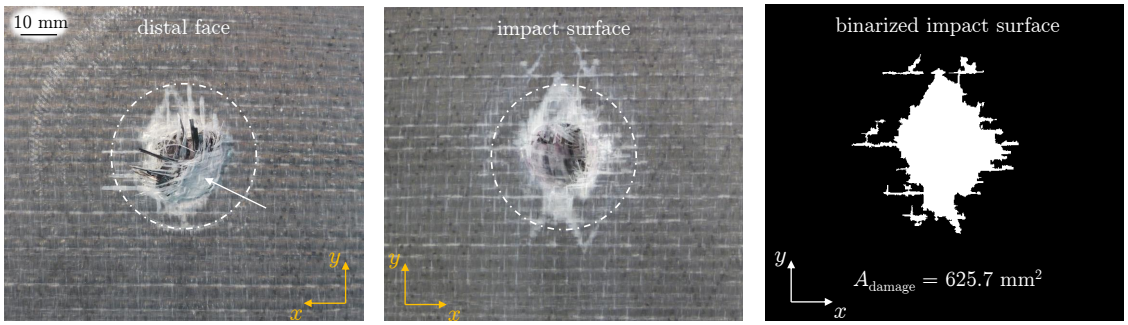
Figure 10: Average values and associated standard deviations of (a) displacement at fibre failure, corresponding to the initiation of the penetration of the sample and, (b) dissipated energy calculated before penetration (sub-critical phase) and total dissipated energy of the baseline and the engineered SRPP/CFPP hybrid composite.

In Figures 11 and 12, photographs taken from the surface of impacted baseline and engineered samples, respectively, reveal that damage (whitening in the figures) was increased by 43% in the engineered configuration with respect the baseline. The threshold used in the binarization process of the impact surface (in Figures 11c and 12c) was the same for engineered and baseline samples.



(a) (b) (c)

Figure 11: Photographs of (a) the back face and (b) the impact face of a baseline impact sample. (c) Binarized image of the impact surface of a baseline impact sample. The white area corresponds to damage.



(a) (b) (c)

Figure 12: Photographs of (a) the back face and (b) the impact face of an engineered impact sample. (c) Binarized image of the impact surface of an engineered impact sample. The white area corresponds to damage.

4. Discussion

4.1. The essential work of fracture of hybrid SRPP/CFPP structures

From the application of the EWF to the baseline SRPP/CFPP cross-ply DEN-T samples (Figure 3), we obtained an estimate of fracture toughness ($w_{\text{essential}}$ = 213 kJ/m^2) and a measure of the energy dissipation capability of the sample, βw_{plastic} = 17.9 MJ/m^3. The latter is associated with the whitening in Figure 4 and includes delamination of the CFPP layers, PP tape plastic deformation, debonding and fibrillation. βw_{plastic} depends on the specimen geometry [28], yet it provides an important measure of the capability of the structure to dissipate energy

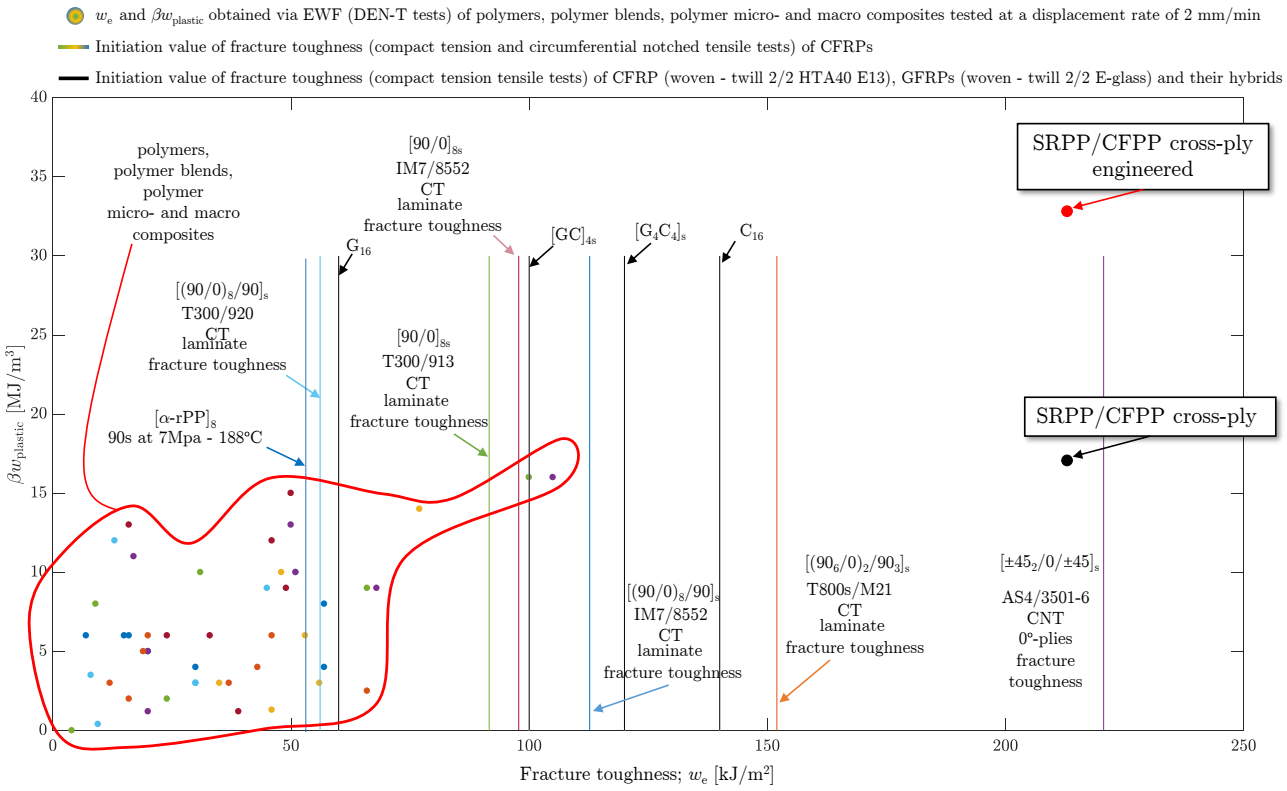


Figure 13: βw_{plastic} vs. $w_{\text{essential}}$ bench-marking of polymers, polymer blends, polymer composites, CF/Epoxy, GF/Epoxy and CF/GF-Epoxy composites. The full coloured dots refer to a large variety of polymers (DEN-T tests at 2 mm/min displacement rate) [3, 28]. The vertical lines refer to the initiation value of fracture toughness for CF/Epoxy composites [25] and CF/Epoxy, GF/Epoxy, CF/GF-Epoxy woven composites [30] (CT/CNT tests). Given the nature of the test, it is not possible to give a measure of βw_{plastic}, which for this data-set has not been reported. The two black and red large circles on the right side of the plot refer to the composites tested in this study.

in a sub-critical way, shielding the ligament plane where critical crack propagation occurs. Therefore, within a design space where damage tolerance is a relevant requirement, high values of both βw_{plastic} and $w_{\text{essential}}$ are desirable.

We compared the baseline configuration with several materials gathered from the literature [3, 25, 28, 30] in Figure 13. In this figure, the x- and y-axis correspond to $w_{\text{essential}}$ and βw_{plastic} respectively. Figure 13 shows that hybridising SRPP with continuous carbon fibres has resulted in a tough material with a good capability of energy dissipation relatively to other materials in the literature.

Further analysis of the damage evolution in a representative baseline sample with

$l = 17$ mm in Figure 4 shows that, prior to the load-drop, strains are highly localised around the notch tip (bright whitening). This has led to the localisation of damage close to the ligament plane and hence, to the abrupt failure of the CFPP plies (load-drop in Figure 4). Therefore, we surmise that the high strain localisation of the baseline microstructure has limited the capability of diffusing damage away from the ligament plane.

4.2. Enhancing the damage diffusion of hybrid SRPP/CFPP structures

In this section we will discuss how engineering the microstructure with tailored laser-cut patterns promotes extensive damage diffusion and increases volumetric energy dissipation.

Figure 5a shows that the engineered microstructure successfully achieved a stable failure process characterised by a gradual stiffness degradation and a load plateau of increasing length with the ligament length. As shown in Figure 7b(i-ii), damage firstly developed in regions far from the ligament plane (high cut density regions); therefore, strain concentrations around the ligament region were successfully delocalised. Then, damage gradually migrated towards the ligament plane as shown in Figures 6 and 7. The resulting extensive damage diffusion protected the ligament plane, thereby delaying final failure. In addition, the DIC maps of Figure 7b reveal that ε_y on the SRPP outer layers never exceeded 17.5%, i.e. about 85% of the failure strain of SRPP [8]. Therefore, we can infer that damage diffusion, in the form of plastic deformation of the PP tape, PP debonding and pull-outs, occurred at a sub-critical level.

The extensive diffused damage has resulted in an increase of about 90% of the slope of the specific work of fracture (w_{fracture}) with respect to the baseline configuration (Figure 8b). Although the slope of w_{fracture} is a geometry-dependent property, we can still use it to compare baseline and engineered samples since the

specimens have the same geometry. Therefore, the increase in slope can be interpreted as an inherent increase in the diffused energy dissipation capability of the structure.

The engineered microstructure increased the diffused energy dissipation (Figure 8a). However, in the samples with engineered microstructure, we do not change the material in the ligament, and hence we expect that the essential work of fracture should not be altered; this is consistent with the experimental observation in Figure 8b.

Using the comparison map of Figure 13, the engineered microstructures shows both high fracture toughness ($w_{\text{essential}}$) and high damage diffusion capability. Therefore, tailoring a pattern of discontinuities in the microstructure has greatly enhanced the damage tolerance of the hybrid SRPP/CFPP composite.

4.3. The role of pull-out of CF bundles in the enhanced energy dissipation of the engineered hybrid SRPP/CFPP structure

In Section 4.2, we discussed the enhanced damage diffusion of the engineered microstructure and the related increase in energy dissipation (90% increase of the slope of w_{fracture} with respect the baseline in Figure 8b). In this section, we will discuss the role of pull-out of CF bundles as the main dissipative mechanism that caused this increase.

As mentioned in Section 2.5, the EWF method assumes that the area of the 'plastic' region (A_{ultimate}) scales with l^2; therefore, $W_{\text{plastic}} \propto l^2$. For the engineered configuration, the volumetric work of fracture (W_{plastic}) results from the contribution of: (i) debonding, plastic deformation and fibrillation of the PP tapes ($W_{\text{plastic,PP}}$) and (ii) pull-outs of carbon fibre bundles (W_{pullout}).

In this work, we can estimate the area of the 'plastic' region contributing to $W_{\text{plastic,PP}}$

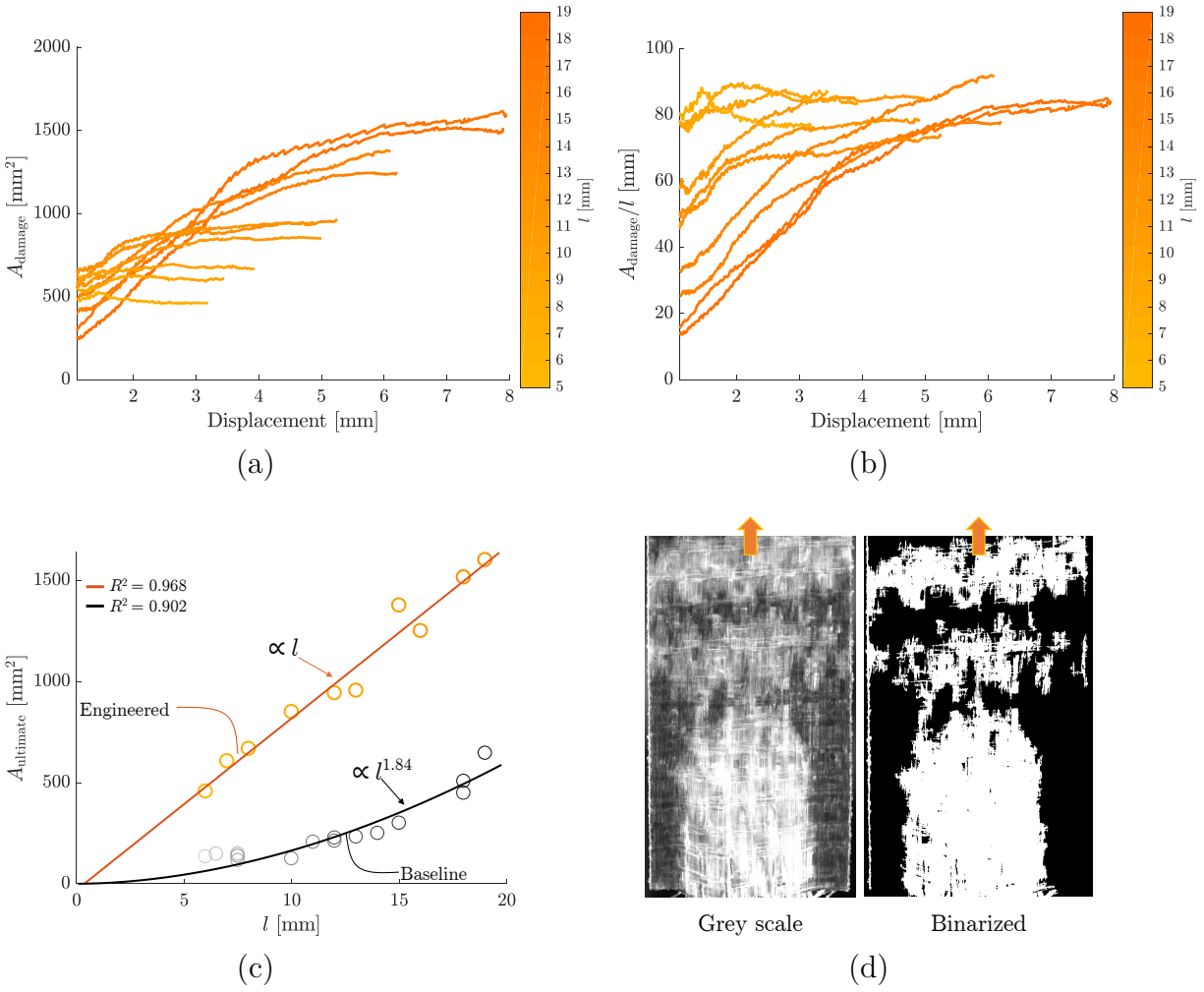


Figure 14: Image analysis of the 'plastic' region of DEN-T samples with engineered microstructure. (a) Area of damage vs. displacement diagrams, (b) Area of damage normalised by the ligament length, (c) ultimate area of damage (calculated at specimen failure) for the engineered and baseline microstructure and (d) example of grey scale image recorded during test and corresponding binarized image. The white area in the binarized image indicates damage.

at each moment during the test, A_{damage}, using the whitened area (due to local debonding, fibrillation and plastic deformation of the PP tapes) observable from the surface of the sample.

We conducted several image analyses of the surface of the samples (Figure 14d) to quantify A_{damage} as a function of the applied displacement (see Figure 14a). As it is shown in Figure 14a, for each sample we report the surface damage from an applied displacement of 1 mm until the final failure. Damage at an applied displacement smaller than 1 mm is not reported because it is affected by the noise in

the image due to the poor contrast between the little damage formed at this early stage and the undamaged region of the sample. In Figure 14b we divided A_{damage} by the respective ligament length. Interestingly, it appears that the curves tend to similar values of A_{ultimate}/l, independently of the ligament length. This implies that, for the samples with engineered microstructure, $A_{\text{ultimate}} \propto l$ (Figure 14c) and therefore, that $W_{\text{plastic,SRPP}} \propto l$. This finding can be explained as follows: the presence of laser-cuts (fixed position along the sample length) delocalises damage which is therefore forced to develop around them. Consequently, being the height of the 'plastic' region bounded by the laser-cuts and therefore independent of the ligament, A_{ultimate} scales linearly with l.

The work done by pull-outs (W_{pullout}) is proportional to the number of laser-cuts involved in the failure process (N_{cuts}) and to the ultimate displacement δ calculated at the sample final failure. Therefore, $W_{\text{pullout}} \propto N_{\text{cuts}} \cdot \delta$. The number of cuts, from which bundles of carbon fibre can be pulled-out, is proportional to l. In addition, given the self-similarity of the load vs. displacement diagrams, $\delta \propto l$ (Figure 5b). Therefore, $W_{\text{pullout}} \propto l^2$.

Combining the analysis conducted in this section ($W_{\text{plastic,PP}} \propto l$ and $W_{\text{pullout}} \propto l^2$) with the results shown in Figure 8b, it becomes clear that the major contribution to the large slope of w_{fracture} vs. l of the engineered microstructure is due to the extensive pull-out of CF bundles.

4.4. Enhancing the impact damage tolerance of hybrid SRPP/CFPP structures

The load vs. displacement diagrams of baseline and engineered microstructures under penetration impact in Figure 9 show that the engineered microstructure succeeded in delaying critical failure (the penetration, which occurs at the peak-load [7]) to larger applied displacement (average increase of 26.6% with respect to the baseline in Figure 10a).

The designed pattern of laser-cuts created a large number of discontinuous CF bundles, each one 16 mm long, thereby locally tailoring the stiffness of the laminate. In addition, the laser-cuts created controlled hot-spots of strain concentrations where sub-critical damage developed in a pre-determined and stable way prior to penetration. This sub-critical damage allowed the laminate to dissipate energy yet preserving its load-bearing capability. Therefore, we surmise that the enhancement in impact damage tolerance of the engineered structure is the result of (i) the locally-tailored stiffness of the composite and (ii) the activation of extensive sub-critical damage.

The examination of the impacted samples in Figures 11 and 12 reveals a larger extent of whitening on the engineered sample — 40% increase on average with respect to the baseline. The larger amount of damage observable from the sample surface correlates well with the average increase of about 42.7% in the energy dissipated at sub-critical levels prior to the peak load (Figure 10b).

5. Conclusions

We tailored laser-cut patterns to engineer the microstructure of a hybrid SRPP/CFPP cross-ply laminate to improve two aspects of its damage tolerance: (i) damage diffusion (i.e. energy dissipation capability) and (ii) impact damage tolerance. With this purpose, we conducted DEN-T and penetration impact tests on a baseline (non-engineered) material and on specimens with engineered microstructures. The main results of this study are summarized below.

Hybridising SRPP with continuous carbon fibre layers resulted in an extremely tough material with laminate fracture toughness values obtained via EWF data reduction of about 213 kJ/m^2.

Introducing artificial discontinuities in SRPP/CFPP hybrid structures under DEN-

T tests has led to:

- delocalising strain concentrations from the notch tip to the laser-cuts. This has promoted extensive sub-critical damage diffusion developing away from the notches resulting in a stable failure process;
- delaying the ultimate failure (occurring at the ligament plane) of the engineered microstructure. For a ligament length $l > 16$ mm, the increase in ultimate failure displacement was: (i) 190% larger than the baseline failure displacement calculated at the unstable crack-growth, occurring at the CFPP failure; and (ii) 50% larger than the baseline ultimate failure displacement calculated at SRPP failure; and
- increasing the energy dissipation capability of the material. The formation of wide-spread pull-outs of CF bundles dissipating energy away from the ligament plane has resulted in an increase of the 'plastic' work (slope of the specific work of fracture) of about 90% with respect to the baseline.

Introducing artificial discontinuities in SRPP/CFPP hybrid structures under penetration impact tests has led to:

- enhancing the impact damage tolerance via a more ductile impact response. The use of tailored laser-cuts led to an increase of 42.5% in energy dissipation at sub-critical levels via formation of damage (PP debonding, fibrillation, plastic deformation and pull-out of carbon fibre bundles) and locally-tailored stiffness;
- delaying the occurrence of critical failure (SRPP fibre failure) to larger indentation depths (increase of 26.6% in deflection at fibre failure); and

Taking the DEN-T and penetration impact results together, we can further conclude that laser-cut patterns can be tailored point-by-point to meet different damage tolerance requirements at different locations within the same structure. This has been achieved using the same technique to engineer the microstructure and

the same material system. Therefore, the technique of introducing discontinuities via laser-cuts provides engineers with a significantly expanded design space and therefore holds the potential to achieve significant industrial impact.

Acknowledgements:

The research leading to these results has been done in the framework of the FiBreMoD project and has received funding from the European Union's Horizon 2020 research and innovation programme under the Marie Skłodowska-Curie grant agreement No 722626. (see www.fibremodproject.eu). Yentl Swolfs acknowledges FWO Flanders for his postdoctoral fellowship. Silvestre Taveira Pinho also acknowledges funding from the EPSRC under grant EP/M002500/1. Jun Tang gratefully acknowledges Prof. Stepan Lomov for guiding his PhD.

[1] Y. Meerten, Y. Swolfs, J. Baets, L. Gorbatikh, I. Verpoest, Penetration impact testing of self-reinforced composites, Composites Part A: Applied Science and Manufacturing 68 (2015) 289–295.

[2] A. Kmetty, T. Bárány, J. Karger-Kocsis, Self-reinforced polymeric materials: A review, Progress in Polymer Science (Oxford) 35 (2010) 1288–1310.

[3] A. Stocchi, V. Pettarin, A. Izer, T. Bárány, T. Czigány, C. Bernal, Fracture behavior of recyclable all-polypropylene composites composed of α- And β-modifications, Journal of Thermoplastic Composite Materials 24 (2011) 805–818.

[4] I. Taketa, J. Ustarroz, L. Gorbatikh, S. V. Lomov, I. Verpoest, Interply hybrid composites with carbon fiber reinforced polypropylene and self-reinforced polypropylene, Composites Part A: Applied Science and Manufacturing 41 (2010) 927–932.

[5] Y. Swolfs, L. Crauwels, E. V. Breda, L. Gorbatikh, P. Hine, I. Ward, I. Verpoest, Tensile behaviour of intralayer hybrid composites of carbon fibre and

self-reinforced polypropylene, Composites Part A: Applied Science and Manufacturing 59 (2014) 78–84.

[6] Y. Swolfs, Y. Meerten, P. Hine, I. Ward, I. Verpoest, L. Gorbatikh, Introducing ductility in hybrid carbon fibre/self-reinforced composites through control of the damage mechanisms, Composite Structures 131 (2015) 259–265.

[7] M. Selezneva, Y. Swolfs, A. Katalagarianakis, T. Ichikawa, N. Hirano, I. Taketa, T. Karaki, I. Verpoest, L. Gorbatikh, The brittle-to-ductile transition in tensile and impact behavior of hybrid carbon fibre/self-reinforced polypropylene composites, Composites Part A: Applied Science and Manufacturing 109 (2018) 20–30.

[8] J. Tang, Y. Swolfs, M. Yang, K. Michielsen, J. Ivens, S. V. Lomov, L. Gorbatikh, Discontinuities as a way to influence the failure mechanisms and tensile performance of hybrid carbon fiber/self-reinforced polypropylene composites, Composites Part A: Applied Science and Manufacturing 107 (2018) 354–365.

[9] Y. Swolfs, J. Shi, Y. Meerten, P. Hine, I. Ward, I. Verpoest, L. Gorbatikh, The importance of bonding in intralayer carbon fibre/self-reinforced polypropylene hybrid composites, Composites Part A: Applied Science and Manufacturing 76 (2015) 299–308.

[10] G. Bullegas, S. T. Pinho, S. Pimenta, Engineering the translaminar fracture behaviour of thin-ply composites, Composites Science and Technology 131 (2016) 110–122.

[11] G. Bullegas, J. Benoliel, P. L. Fenelli, S. T. Pinho, S. Pimenta, Towards quasi isotropic laminates with engineered fracture behaviour for industrial applications, Composites Science and Technology 165 (2018) 290–306.

[12] F. Narducci, S. T. Pinho, Exploiting nacre-inspired crack deflection mechanisms in CFRP via micro-structural design, Composites Science and Technology 153 (2017) 178–189.

[13] F. Narducci, S. T. Pinho, Interaction between nacre-like CFRP mesolayers and long-fibre interlayers, Composite Structures 200 (2018) 921–928.

[14] F. Narducci, K.-Y. Lee, S. Pinho, Realising damage-tolerant nacre-inspired CFRP, Journal of the Mechanics and Physics of Solids 116 (2018) 391–402.

[15] G. Czél, M. Jalalvand, M. R. Wisnom, Demonstration of pseudo-ductility in unidirectional hybrid composites made of discontinuous carbon/epoxy and continuous glass/epoxy plies, Composites Part A: Applied Science and Manufacturing 72 (2015) 75–84.

[16] G. Czél, S. Pimenta, M. Wisnom, P. Robinson, Demonstration of pseudo-ductility in unidirectional discontinuous carbon fibre/epoxy prepreg composites, Composites Science and Technology 106 (2015) 110–119.

[17] K. B. Broberg, Crack-growth criteria and non-linear fracture mechanics, Journal of the Mechanics and Physics of Solids 19 (1971) 407–418.

[18] K. B. Broberg, On stable crack growth, Journal of the Mechanics and Physics of Solids 23 (1975) 215–237.

[19] K. B. Broberg, Critical review of some methods in nonlinear fracture mechanics, Engineering Fracture Mechanics 50 (1995) 157–164.

[20] Y. Mai, S. Wong, X. Chen, Application of fracture mechanics for characterization of toughness of polymer blends, in: D. Paul, C. Bucknall (Eds.), Polymer blends: formulations and performance, Vol 2., Wiley, New York, 2000, pp. 17–58.

[21] Y. Swolfs, L. Crauwels, L. Gorbatikh, I. Verpoest, The influence of weave architecture on the mechanical properties of self-reinforced polypropylene, Composites Part A: Applied Science and Manufacturing 53 (2013) 129–136.

[22] P. J. Hine, R. H. Olley, I. M. Ward, The use of interleaved films for optimising the production and properties of hot compacted, self reinforced polymer composites, Composites Science and Technology 68 (2008) 1413–1421.

[23] P. J. Hine, A. P. Unwin, I. M. Ward, The use of an interleaved film for optimising the properties of hot compacted polyethylene single polymer composites, Polymer 52 (2011) 2891–2898.

[24] S. T. Pinho, P. Robinson, L. Iannucci, Fracture toughness of the tensile and compressive fibre failure modes in laminated composites, Composites Science and Technology 66 (2006) 2069–2079.

[25] M. J. Laffan, S. T. Pinho, P. Robinson, A. J. McMillan, Translaminar fracture toughness testing of composites: A review, Polymer Testing 31 (2012) 481–489.

[26] J. Tang, A. Aslani, Y. Swolfs, G. Bullegas, S. T. Pinho, S. V. Lomov, L. Gorbatikh, Exploring discontinuities and hybridization to design gradual failure in unidirectional carbon fibre/self-reinforced polypropylene composites, in: 21st International Conference on Composite Materials.

[27] G. Bullegas, S. T. Pinho, S. Pimenta, High-Toughness CFRP Laminates with Engineered Fracture Surfaces: A Shark-Teeth Design, American Society for Composites Thirty-First Technical Conference (2016).

[28] T. Bárány, T. Czigány, J. Karger-Kocsis, Application of the essential work of fracture (EWF) concept for polymers, related blends and composites: A review, Progress in Polymer Science 35 (2010) 1257–1287.

[29] R. Hill, On discontinuous plastic states, with special reference to localized necking in thin sheets, Journal of the Mechanics and Physics of Solids 1 (1952) 19–30.

[30] Y. Swolfs, Y. Geboes, L. Gorbatikh, S. T. Pinho, The importance of translaminar fracture toughness for the penetration impact behaviour of woven carbon/glass hybrid composites, Composites Part A: Applied Science and Manufacturing 103 (2017) 1–8.